SIAM J. NUMER. ANAL.
Vol. 55, No. 4, pp. 1719–1739

ON HANGING NODE CONSTRAINTS FOR NONCONFORMING FINITE ELEMENTS USING THE DOUGLAS–SANTOS–SHEEN–YE ELEMENT AS AN EXAMPLE*

WOLFGANG BANGERTH†, IMBUNM KIM‡, DONGWOO SHEEN‡, AND JAERYUN YIM§

Abstract. On adaptively refined quadrilateral or hexahedral meshes, one usually employs *constraints* on degrees of freedom to deal with hanging nodes. How these constraints are constructed is relatively straightforward for *conforming* finite element methods: The constraints are used to ensure that the discrete solution space remains a subspace of the continuous space. On the other hand, for *nonconforming* methods, this guiding principle is not available and one needs other ways of ensuring that the discrete space has desirable properties. In this paper, we investigate how one would construct hanging node constraints for nonconforming elements, using the Douglas–Santos–Sheen–Ye (DSSY) element as a prototypical case. We identify three possible strategies, two of which lead to provably convergent schemes with different properties. For both of these, we show that the structure of the constraints differs qualitatively from the way constraints are usually dealt with in the conforming case.

Key words. finite element method, adaptive meshes, hanging nodes, constraints

AMS subject classifications. 65N30, 65N16, 65N50

DOI. 10.1137/16M1071432

1. Introduction.

Refining individual cells of a finite element mesh — for example, in adaptive mesh refinement schemes based on error estimators — creates faces with so-called hanging nodes, i.e., vertices that are located in the interior of edges or faces of some of the surrounding elements. On such faces, shape functions cannot easily be defined without losing some of the properties of the finite element space that are necessary to show convergence at the appropriate order. However, there are well-known strategies for resolving this problem, either through the use of transition elements that entirely remove the hanging nodes (for example, in the red-green refinement strategy for triangles; see [5]), or through the use of constraints on degrees of freedom that ensure that the critical property of the finite element necessary for the theory is restored [16, 5, 19, 20]. While both of these approaches can easily be used for triangular or tetrahedral meshes, a lack of practical and widely

*Received by the editors April 19, 2016; accepted for publication (in revised form) February 16, 2017; published electronically July 13, 2017.
http://www.siam.org/journals/sinum/55-4/M107143.html
Funding: The work of the first author was supported by the National Science Foundation through award OCI-1148116 and by the Computational Infrastructure in Geodynamics (CIG) initiative, through the National Science Foundation under award EAR-0949446, and the University of California–Davis. The work of the first and third author's was supported in part by National Research Foundation of Korea NRF-2014R1A2A1A11052429. The work of the third author was also supported by the Next-Generation Information Computing Development Program through the National Research Foundation of Korea (NRF) funded by the Ministry of Education, Science and Technology (NRF-2015M3C4A7065662).
†Department of Mathematics, Colorado State University, Fort Collins, CO 80523 (bangerth@colostate.edu).
‡Department of Mathematics, Seoul National University, Seoul 08826, Republic of Korea, and Interdisciplinary Program in Computational Science and Technology, Seoul National University, Seoul 08826, Republic of Korea (ibkim11@gmail.com, dongwoosheen@gmail.com).
§Interdisciplinary Program in Computational Science and Technology, Seoul National University, Seoul 08826, Republic of Korea (jaeryun.yim@gmail.com).

used transition element strategies requires the use of constraints for quadrilateral and hexahedral meshes.

When using conforming finite elements, the construction of these constraints is typically straightforward: we use the constraints to restore the conformity property for the finite element space. For example, for H^1-conforming elements, one needs to restore the *continuity* of the finite element space along the affected face with a hanging node. In the case of conforming bilinear elements, this implies the familiar constraint that a degree of freedom U_H defined on a hanging node needs to satisfy $U_H = \frac{1}{2}U_L + \frac{1}{2}U_R$, where U_L, U_R are the degrees of freedom defined at the ends of the parent edge on which the hanging node lives. Similar constructions are used for $H(\mathrm{curl})$- and $H(\mathrm{div})$-conforming elements where constraints are used to enforce the continuity of tangential or normal components of the finite element field, respectively.

On the other hand, the situation is not so clear for nonconforming elements. There, the discrete finite element space is already nonconforming with regard to the continuous solution space, even on meshes without hanging nodes. Consequently, there is no point in restoring conformity along faces with hanging nodes, and conformity will not be useful as the guiding principle for construction of constraints. At the same time, nonconforming elements—sitting somewhere between conforming and entirely discontinuous elements—have enough internal structure that they do not need the addition of penalty terms to the bilinear form, as is necessary, for example, for the discontinuous Galerkin (DG) method. Consequently, the guiding principle should be to come up with *some* kind of constraint at hanging nodes that restores the critical property of the discrete space that allows us to avoid penalty terms.

In this contribution, we investigate this situation for the nonconforming Douglas–Santos–Sheen–Ye (DSSY) element [12] that can be used in the discretization of the Laplace and related equations. The DSSY element provides optimal convergence order, but because its degrees of freedom are defined on the faces of cells rather than their vertices, it has a smaller stencil and consequently sparser system matrix than the regular, H^1-conforming Lagrange elements. Based on analogies with other elements and knowledge of the proof of convergence of the DSSY element, we will introduce three possible ways to construct constraints at hanging nodes. While the most obvious choice (later called "option A") turns out to not be convergent, the other two approaches are in fact convergent. One of these ("option B") is built in such a way that it restores the critical ingredient in the original proof of optimal convergence found in [12]. However, this construction of constraints does not just couple degrees of freedom located on the face with the hanging node (as is the case for all conforming elements we are aware of) but indeed *all* degrees of freedom on the entire larger cell. Because these may in turn be constrained themselves, the stencil of constrained degrees of freedom may in fact extend far beyond a cell and its immediate neighbors. This has significant implications for implementations that we will discuss as well. To address this problem, we investigate a weaker, alternative choice ("option C") of constraints that does not share this drawback but requires more work to prove convergence.

The remainder of this paper is structured as follows. Section 2 provides an overview of the DSSY element, and section 3 introduces further notation necessary in the discussions that follow. Section 4 then traces out the proof of convergence on meshes without hanging nodes and in particular points out the critical pieces that get lost if a mesh does have hanging nodes; it also presents three possible constructions of constraints that could reasonably be used at hanging nodes. Sections 5 and 6 then cover the analysis of the two alternative constructions that are in fact convergent,

followed by numerical examples in section 7 that quantitatively assess the options previously identified. We conclude in section 8.

Remark 1.1. While our discussions herein are based specifically on the DSSY element, we intend the construction of constraints for this element to also provide guidance for other nonconforming elements, such as the simplicial Crouzeix–Raviart element [9] or the quadrilateral Rannacher–Turek element [15], for which we believe that similar principles will apply.

Our discussions below will be restricted to two dimensions because the degree of notation, as well as the graphics necessary to build intuition, would be too cumbersome without providing additional insight. However, the extension of our work to three dimensions is obvious.

Remark 1.2. Neither nonconforming elements nor adaptively refined meshes using hanging nodes are new. As a consequence, it is perhaps surprising that we have not been able to find much literature on their combination. Carstensen and Hu [6] make an assumption that is equivalent to option C discussed in section 4.2 but do not discuss alternatives, or elaborate on practical implications of this assumption. Huang and Xie [13] also use a similar assumption, but in the context of avoiding hanging node constraints when dealing with *conforming* elements at hanging nodes.

Finally, one of the reviewers of this paper pointed out the Ph.D. thesis of Schmid [17]. The thesis was published as a book (in German), is now out of print, and is consequently difficult to access. We have not been able to verify that it contains material related to our work, though we do not doubt it. An earlier paper by Schmid and Wagner [18, section 4.3] has a remark that states that nodes on hanging edges need to be treated differently from those on regular edges—a statement that at the time may not have been as obvious as it appears today; it does not, however, provide details on how *specifically* this treatment should look, nor any analysis.

2. A brief overview of the DSSY element. The DSSY element [12] was developed for the discretization of second-order elliptic problems such as the Poisson equation:

$$-\Delta u = f \qquad \text{in } \Omega, \tag{2.1a}$$

$$u = g \qquad \text{on } \partial\Omega. \tag{2.1b}$$

For these equations, the appropriate solution space is $V = H^1(\Omega)$. As a typical nonconforming finite element discretization, the DSSY element defines a finite dimensional space V_h that does not satisfy the usual condition $V_h \subset V$. Rather, it contains functions that are discontinuous and consequently not members of V.

More specifically, the DSSY element is defined as follows [4, 12]. Let $\widehat{K} = [-1, 1]^2$ be the reference element and $\mathbb{T} = \{K\}$ a subdivision of Ω into quadrilaterals that are mapped from the reference cell by bilinear mappings ϕ_K. The DSSY space $\widehat{V}$ is then defined on the reference cell as

$$\widehat{V} = \operatorname{span}\{1, \widehat{x}_1, \widehat{x}_2, \theta(\widehat{x}_1) - \theta(\widehat{x}_2), \widehat{x}_1\widehat{x}_2\}, \tag{2.2}$$

where θ can be defined as either

$$\theta(\xi) = \xi^2 - \frac{5}{3}\xi^4 \qquad \text{or} \qquad \theta(\xi) = \xi^2 - \frac{25}{6}\xi^4 + \frac{7}{2}\xi^6.$$

The choice of these options will be immaterial to the remainder of this paper, but the additional quartic or sextic term enables the finite element space $\widehat{V}$ to fulfill the mean

value property[1]

$$\widehat{v}(\widehat{\mathbf{m}}_{\widehat{e}}) = \fint_{\widehat{e}} \widehat{v} \tag{2.3}$$

for all edges $\widehat{e}$ of the reference cell $\widehat{K}$; $\widehat{\mathbf{m}}_{\widehat{e}}$ denotes the center point of edge $\widehat{e}$. Here, and in what follows, $\fint_s f = \frac{1}{|s|}\int_s f$ denotes the average Lebesgue integral of f over s. The addition of the last shape function in the definition (2.2) (which leads to an interior bubble function when choosing a set of dual functionals for $\widehat{V}$) is necessary to guarantee the optimal convergence order on general quadrilateral meshes if these shape functions are mapped from a standard reference cell (see [4, 12]); it can be omitted on meshes consisting only of parallelograms.[2]

This space cannot be connected in a continuous way across cells to form a global space sufficiently rich to approximate the solutions of partial differential equations. Rather, the DSSY construction only requires that the mean values of functions are equal on interfaces γ between neighboring cells $K(\gamma)^+$ and $K(\gamma)^-$. One can equivalently require continuity at edge midpoints, but using the viewpoint of equality of mean values will turn out to yield easier-to-understand insights during the proofs below; we will therefore base our arguments on this perspective.

If we define $\mathcal{E}^i$ to be the set that consists of all interior edges of the mesh, and assuming we have a mesh without hanging nodes, then we can construct the global space as follows:

$$V_h(\mathbb{T}) = \left\{ u_h \in L^2(\Omega) \,\middle|\, u_h \circ \phi_K \in \widehat{V}\ \forall K \in \mathbb{T}, \fint_e [u_h]_e = 0\ \forall e \in \mathcal{E}^i \right\}. \tag{2.4}$$

The dual node functionals that define the finite element basis (and consequently the degrees of freedom; see [2]) for this space are given by the integral averages

$$\psi_e(\varphi_h) = \fint_e \varphi_h \qquad \forall e \in \mathcal{E}^i, \tag{2.5a}$$

$$\psi_K(\varphi_h) = \fint_K \varphi_h w_K \qquad \forall K \in \mathbb{T}, \tag{2.5b}$$

where the function $w_K(\mathbf{x})$ is the pushed-forward version of the weight $\widehat{x}_1\widehat{x}_2$ on the reference cell $\widehat{K} = [-1,1]^2$ under the mapping $\phi_K : \widehat{K} \to K$.

3. Further notation. In the sections below, we will discuss how to extend the definitions of the previous section to the case of meshes $\mathbb{T}$ with hanging nodes. To this end, let us introduce the notation we will require below.

Triangulation. Let $\mathbb{T}_0$ be a regular triangulation on Ω which consists of quadrilaterals so that two closed cells $K_1, K_2 \in \mathbb{T}_0$ either share a common vertex, a complete edge, are identical, or do not touch at all. We can then refine it recursively into the target triangulation $\mathbb{T} = \mathbb{T}_N$ by ensuring that $\mathbb{T}_n$ results from $\mathbb{T}_{n-1}$ by regular bisection in both directions of a subset of cells, and ensuring that neighboring cells never differ by more than one refinement level (i.e., each edge has at most one hanging vertex).

[1] In the case of Rannacher–Turek element [15], one chooses $\theta(\xi) = \xi^2$. However, for this choice, (2.3) does not hold.

[2] Instead of the parametric version of the DSSY element introduced above, there is also a non-parametric version with four degrees of freedom [14] such that the mean value property (2.3) holds for general quadrilaterals and optimal convergence is attained.

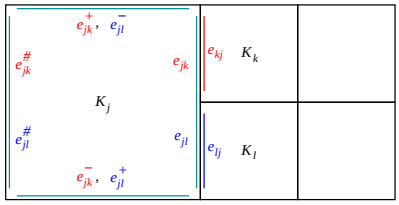

FIG. 1. *Local notation for edges on cells with a hanging edge. Superscripts* $\#, +$, *and* $-$ *to* e_{jk} *denote the edges of* K_j *that lie opposite to* e_{jk}, *that share a vertex with* e_{kj}, *and that do not share a vertex with* e_{kj} *but are also not opposite to* e_{jk}, *respectively, and similarly for the superscripted versions of* e_{jl}. *Note the equivalences* $e_{jk}^{\#} = e_{jl}^{\#}, e_{jk}^{+} = e_{jl}^{-}, e_{jk}^{-} = e_{jl}^{+}, e_{jk} = e_{jl}$.

Vertices and edges. For any element $K \in \mathbb{T}$, let $\mathcal{N}(K)$ denote its vertices, and $\mathcal{E}(K)$ its edges. The sets of all nodes and edges in the triangulation $\mathbb{T}$ are denoted by $\mathcal{N} := \cup_{K\in\mathbb{T}}\mathcal{N}(K)$ and $\mathcal{E} := \cup_{K\in\mathbb{T}}\mathcal{E}(K)$, respectively. Furthermore, the sets of all interior and boundary nodes and edges are designated by $\mathcal{N}^i, \mathcal{N}^b, \mathcal{E}^i$, and $\mathcal{E}^b$, respectively.

Hanging edges and nodes. We call places where cells of different refinement levels come together (see Figure 1) *hanging edges* and the single vertex at their midpoints *hanging nodes*. In order to concisely define the finite element space $V_h(\mathbb{T})$ on meshes with hanging edges, we will need the following terms:

1. (Generation and descendant neighbors) Given an element $K \in \mathbb{T}$ which is obtained by (recursive) refinement from element $K_0 \in \mathbb{T}_0$, let the *generation of* K, denoted by $\mathrm{Gen}(K)$, be the number of bisection steps required to go from K_0 to K [7]. A cell $K' \in \mathbb{T}$ is called a *descendant neighbor* of K if K' and K are adjacent and $\mathrm{Gen}(K') > \mathrm{Gen}(K)$. The one-hanging-node-per-edge rule guarantees that for any two neighbors K and K', we have that $\mathrm{Gen}(K') - \mathrm{Gen}(K) \in \{-1, 0, 1\}$.
2. (Hanging nodes) A vertex $\mathbf{z} \in \mathcal{N}^i$ is called a *hanging node* if there exists an element $K \in \mathbb{T}$ such that $\mathbf{z} \in \partial K \backslash \mathcal{N}(K)$. We will denote by $\mathcal{N}_H$ the set of all hanging nodes and by $\mathcal{N}_R := \mathcal{N}^i \setminus \mathcal{N}_H$ the set of all regular (interior) nodes.
3. (Hanging edges) An edge $e \in \mathcal{E}^i$ is called a *hanging edge* if there exists a hanging node $\mathbf{z} \in e$ that is not one of the end points of e. An edge $e' \in \mathcal{E}^i$ is called a child edge if there exists a hanging edge e such that $e' \cap e \neq \emptyset$. We will denote by $\mathcal{E}_H$ the set of all hanging edges, $\mathcal{E}_C$ the set of child edges, and $\mathcal{E}_R := \mathcal{E}^i \backslash (\mathcal{E}_H \cup \mathcal{E}_C)$ the set of regular edges.
4. (Local description of hanging edge) Let e_{jk} be the edge of cell K_j adjacent to a neighboring cell K_k. If $e_{jk} \in \mathcal{E}_R$, then e_{jk} is also a complete edge e_{kj} of cell K_k. On the other hand, suppose two elements $K_j, K_k \in \mathbb{T}$ are adjacent such that K_k is a descendant neighbor to K_j; then $e_{jk} \in \mathcal{E}_H$ and $e_{kj} \in \mathcal{E}_C$.

We note that hanging nodes are conceptually part of small cells along refined edges, whereas hanging edges belong to the large cells. We also remark that $\mathcal{E}^i$ is the disjoint union of $\mathcal{E}_R, \mathcal{E}_H$, and $\mathcal{E}_C$ and that $\mathcal{N}^i$ is the disjoint union of $\mathcal{N}_R$ and $\mathcal{N}_H$. We consider regular nodes $\mathcal{N}_R$ and edges $\mathcal{E}_R$ to be subsets of the *interior* nodes $\mathcal{N}^i$ and edges $\mathcal{E}^i$ only since boundary nodes and edges will not be of any concern in the following.

We introduce further notation convention as follows. Let e_{jk} be a hanging edge. Then let $e_{jk}^{\#}$ denote the edge of K_j which lies opposite to e_{jk}. Among the remaining

two edges of K_j, let e_{jk}^+ and e_{jk}^- be the edges that do and do not share a vertex with e_{kj}, respectively (see Figure 1 for an illustration). It is worth noting that an edge of cell K_j can be denoted in several different ways depending on which of its neighbors we currently consider.

Spaces and norms. Let S be a bounded open domain in $\mathbb{R}^2$. Denote $L^2(S)$ and $H^1(S)$ the standard Sobolev spaces on S with the standard norms $\|\cdot\|_{0,S}$ and $\|\cdot\|_{1,S}$. $H_0^1(S)$ is the subspace of $H^1(S)$ consisting of functions whose trace on ∂S is zero. Note that the standard seminorm $|\cdot|_{1,S}$ is a norm on $H_0^1(S)$ provided that the boundary of S is sufficiently smooth. $(\cdot,\cdot)_S$ and $\langle\cdot,\cdot\rangle_{\partial S}$ denote the $L^2(S)$ and $L^2(\partial S)$ inner products, respectively. If $S = \Omega$, the subscript Ω on norms and inner products will be omitted.

Averages and jumps. Let ω be a two- or one-dimensional measurable subset with $|\omega| > 0$. For $u \in L^1(\omega)$, denote by $\fint_\omega u := \frac{1}{|\omega|}\int_\omega u$ the average integral value of u on ω. On an edge $e_{jk} \in \mathcal{E}^i$, we define the jump $[u]_{e_{jk}}$ of u on e_{jk} by

$$[u]_{e_{jk}} := u|_{K_k} - u|_{K_j}\,.$$

Note that the jump $[u]_{e_{jk}}$ depends not only on the location of the edge but also on its direction. In particular, $[u]_{e_{kj}} = -[u]_{e_{jk}}$. For an edge e_j of K_j on $\partial\Omega$, we define $[u]_{e_j} := -\,u|_{K_j}$. We will occasionally write $[u]_e$ and omit the subscript of the edge direction if the jump (or an integral of it) across an edge e is zero.

Throughout this paper, C denotes a generic constant for inequalities. The mesh parameter h is defined by $h := \max_{K\in\mathbb{T}} \operatorname{diam}(K)$.

4. Discretization with the DSSY element. We will use the Poisson equation (2.1a)–(2.1b) to illustrate how we discretize partial differential equations using the DSSY element described in section 2 and how this informs our approach for constructing hanging node constraints for situations such as those described in section 3. Because the choice of boundary values are immaterial to the discussion herein, let us assume for simplicity that we use homogeneous Dirichlet boundary conditions, i.e., $g = 0$. Then recall that the weak form of problem (2.1) requires us to find $u \in V_0 = H_0^1(\Omega)$ so that

$$a(u,v) = (f,v) \qquad \forall v \in V_0, \tag{4.1}$$

where $a(u,v) = (\nabla u, \nabla v) = \int_\Omega \nabla u \cdot \nabla v \,\mathrm{d}\mathbf{x}$.

The nonconforming Galerkin approximation to (4.1) is to find $u_h \in V_{h,0} = V_{h,0}(\mathbb{T})$ so that

$$a_h(u_h,v_h) = (f,v_h) \qquad \forall v_h \in V_{h,0}. \tag{4.2}$$

Here, $V_{h,0}(\mathbb{T})$ is the space of all functions in $V_h(\mathbb{T})$ that have mean value zero on each boundary face $e \in \mathcal{E}^b$ of the mesh, and

$$a_h(u_h,v_h) = \sum_{K\in\mathbb{T}} (\nabla u_h, \nabla v_h)_K. \tag{4.3}$$

For future use, let us also define the broken energy norm for functions $v \in V_h(\mathbb{T}) + H^1(\Omega)$ that is associated with this bilinear form by

$$|||v|||_h = \sqrt{a_h(v,v)}.$$

4.1. Key steps in a priori error estimates on regular meshes. Unlike for entirely discontinuous finite element spaces, the structure of V_h allows us to solve this problem without the need for additional penalty terms to treat the discontinuity of functions in V_h. However, error estimates incur a "nonconformity penalty" [21]. Consequently, if there are no hanging nodes in the mesh, the energy norm error of the numerical solution consists of the usual best-approximation error plus the penalty and is bounded as follows:

$$|||u-u_h|||_h \le C\left(\inf_{\varphi_h\in V_h}|||u-\varphi_h|||_h + \sup_{w_h\in V_h}\frac{a_h(u,w_h)-(f,w_h)}{|||w_h|||_h}\right). \tag{4.4}$$

For the purposes of this paper, the first of the two terms on the right-hand side is not important as we know that it is of optimal order [12]. However, it is necessary to understand the details of the second term as it will inform us about the properties we will need of the discrete space in the presence of hanging nodes if we want to ensure optimality of the convergence order. Integrating its numerator by parts on each cell and using the strong form (2.1) of the equation, we see that

$$\begin{aligned} a_h(u,w_h)-(f,w_h) &= \sum_K (\nabla u,\nabla w_h)_K - (f,w_h)_K \\ &= \sum_K (-\Delta u - f, w_h)_K + \langle \mathbf{n}_K\cdot\nabla u, w_h\rangle_{\partial K} \\ &= -\sum_{e\in\mathcal{E}^i}\langle \mathbf{n}_e\cdot\nabla u, [w_h]_e\rangle_e\,. \end{aligned}$$

Here, $\mathbf{n}_K$ is the unit outward normal to cell K, and $\mathbf{n}_e$ denotes the unit normal vector to edge e with a direction consistent with that chosen for the jump $[w_h]_e$.

Because the jump $[w_h]_e$ of a function $w_h\in V_h$ is zero on average (see (2.4)), we can subtract any constant from $\mathbf{n}_e\cdot\nabla u$ and leave the result unchanged. Specifically, denoting $\overline{\mathbf{g}}_e = \fint_e \nabla u$, we get

$$\begin{aligned} |a_h(u,w_h)-(f,w_h)| &\le \sum_{e\in\mathcal{E}_i} |\langle \mathbf{n}_e\cdot(\nabla u-\overline{\mathbf{g}}_e), [w_h]_e\rangle_e| \\ &\le \sum_{e\in\mathcal{E}_i} \|\nabla u-\overline{\mathbf{g}}_e\|_{0,e}\|[w_h]_e\|_{0,e}. \end{aligned}$$

Standard polynomial interpolation estimates imply that

$$\left(\sum_{e\in\mathcal{E}_i}\|\nabla u-\overline{\mathbf{g}}_e\|_{0,e}^2\right)^{1/2} \le Ch^{1/2}\|u\|_{H^2(\Omega)}, \tag{4.5a}$$

$$\left(\sum_{e\in\mathcal{E}_i}\|[w_h]_e\|_{0,e}^2\right)^{1/2} \le Ch^{1/2}|||w_h|||_h. \tag{4.5b}$$

Consequently, $|a_h(u,w_h)-(f,w_h)| \le Ch\|u\|_{H^2(\Omega)}|||w_h|||_h$, and (4.4) provides us with an optimal convergence order in the broken H^1 norm: $|||u-u_h|||_h \le Ch\|u\|_{H^2(\Omega)}$.

4.2. Options for extensions to locally refined meshes. Given these arguments, the question before us is how we need to extend definition (2.4) of the finite element space $V_h(\mathbb{T})$ to the case of meshes with hanging nodes. Our experience with how this is done for conforming elements, as well as the critical pieces of the theory outlined above, has led us to three possible options that we will illustrate with the notation of Figure 1:

A. Require that

$$\fint_{e_{kj}} w_h = \fint_{e_{jk}} w_h \qquad \text{and} \qquad \fint_{e_{lj}} w_h = \fint_{e_{jk}} w_h, \tag{4.6}$$

i.e., that the average of a function w_h on every small edge e_{kj}, e_{lj} equals the average on the long edge $e_{jk} = e_{jl}$.

This approach constructs constraints that only involve degrees of freedom defined on the parent edge and its children. However, it does not provide the key property that $\fint_e [w_h]_e = 0$ for all edges: while it is true for regular edges $e \in \mathcal{E}_R$ and parent edges $e \in \mathcal{E}_H$ as a whole, it does not hold for individual child edges $e \in \mathcal{E}_C$.

The constraint in (4.6) can be interpreted as constraining the degrees of freedom on the child edges against the degree of freedom on the hanging (parent) edge. This is how constraints are typically written for conforming elements and would allow the use of algorithms and data structures that are already implemented in common finite element packages. Disappointingly, however, this advantageous property is entirely negated by the fact that this choice of constraint construction does not lead to a convergent scheme (see section 7).

B. Require that

$$\fint_{e_{kj}} [w_h]_{e_{kj}} = 0, \qquad \fint_{e_{lj}} [w_h]_{e_{lj}} = 0. \tag{4.7}$$

Here, the average jump $\fint_e [w_h]_e = 0$ is zero on all child edges individually and consequently also on all parent edges. We therefore know that the solution satisfies the properties required in establishing the a priori error estimates outlined above, and the convergence proof follows trivially. This formulation of constraints allows the values on child edges to be different and therefore imposes a weaker constraint than the first approach above.

Unfortunately, as we will show in the following section, the constraints constructed this way couple not only degrees of freedom on a parent edge and its children but in fact *all* degrees of freedom on a large cell with those on children of its edges. This can then lead to chains of constraints that propagate beyond a single cell and consequently requires significantly more complicated data structures and algorithms than the "usual" cases encountered with conforming elements.

C. Require that

$$\frac{1}{2}\left\{ \fint_{e_{kj}} w_h + \fint_{e_{lj}} w_h \right\} = \fint_{e_{jk}} w_h, \tag{4.8}$$

i.e., the average of the averages on the child edges equals the average on the large edge. This statement is weaker than the one used in (4.7) and can be interpreted as constraining the degree of freedom on a *parent* edge against the two values on the child edges, in a reversion of the way we usually build hanging node constraints.

As we will show below, this approach constructs constraints only coupling shape functions corresponding to degrees of freedom located on the parent edge and its children. It does not satisfy the property $\fint_e [w_h]_e = 0$ for individual child edges $e \in \mathcal{E}_C$, and consequently we will have to work harder to prove convergence.

As we will see numerically in section 7, the first of these three choices results in a suboptimal convergence order on meshes with hanging nodes. We will therefore not consider it in any more detail. The second and third turn out to be largely comparable in accuracy, though option B seems to create smaller L_2 errors in some circumstances. On the other hand, as already mentioned above, option B has more severe *practical* consequences in implementations and consequently may be computationally more expensive. We will therefore consider both options B and C in more theoretical and practical detail in the following two sections; we start with option B since its analysis is less involved.

Remark 4.1. None of the three options above inherently rely on the fact that refinement of cells is done by equal bisection of cells into four children. Rather, the formulas are easily adapted to the case where one refines a cell into 3×3 children, or where edges are not bisected at their midpoints. This would, for example, facilitate the construction of graded meshes refined toward boundary or internal layers.

Remark 4.2. The approaches above all incorporate the treatment of hanging nodes into the strong formulation of the discrete problem, i.e., by adjusting the finite dimensional space. There are, however, alternative approaches. For example, one can add penalty terms—in the style of DG methods—for hanging edges only (see, e.g., [11]). These approaches are not of interest to the current paper, however.

5. Extending the DSSY space to meshes with hanging nodes and edges: Option B. The discussions of the previous section motivate us to analyze in more detail the three options for defining the nonconforming space $V_h(\mathbb{T})$ in the presence of hanging nodes. We will start with the second of the three options (see (4.7)), as this turns out the simplest in terms of its convergence theory. It leads to the following space on meshes with hanging nodes and edges:

$$V_h(\mathbb{T}) = \Big\{ u_h \in L^2(\Omega) \,\Big|\, u_h \circ \phi_K \in \widehat{V} \ \forall K \in \mathbb{T},$$

$$\fint_e [u_h]_e = 0 \ \forall e \in (\mathcal{E}_R \cup \mathcal{E}_C) \Big\}, \tag{5.1a}$$

$$V_{h,0}(\mathbb{T}) = \Big\{ u_h \in V_h(\mathbb{T}) \,\Big|\, \fint_e u_h = 0 \ \forall e \in \mathcal{E}^b \Big\}. \tag{5.1b}$$

In analogy to (2.5a) and (2.5b), we can define dual functionals

$$\psi_e(\varphi_h) = \fint_e \varphi_h \ \forall e \in (\mathcal{E}_R \cup \mathcal{E}_H) \tag{5.2}$$

and ψ_K as defined in (2.5b). These then induce a basis $\{\varphi_j\}_{j=1,\dots,\dim(V_{h,0}(\mathbb{T}))}$ for $V_{h,0}(\mathbb{T})$.

We can compute the dimensions of the spaces so defined as follows.

LEMMA 5.1. *The dimension of $V_h(\mathbb{T})$ is equal to $|\mathcal{E}_R| + |\mathcal{E}_H| + |\mathcal{E}^b| + |\mathbb{T}|$. The dimension of $V_{h,0}(\mathbb{T})$ is equal to $|\mathcal{E}_R| + |\mathcal{E}_H| + |\mathbb{T}|$.*

Proof. Since the space $\widehat{V}$ defined in (2.2) has dimension five, the space

$$V_h^{\mathrm{DG}}(\mathbb{T}) = \Big\{ u_h \in L^2(\Omega) \,\Big|\, u_h \circ \phi_K \in \widehat{V} \ \forall K \in \mathbb{T} \Big\}$$

has dimension $5|\mathbb{T}|$. Because every regular edge $e \in \mathcal{E}_R$ is part of two cells whereas every edge in $\mathcal{E}_H, \mathcal{E}_C, \mathcal{E}^b$ is only part of one cell, and because every cell K has four

edges, we know that $4|\mathbb{T}| = 2|\mathcal{E}_R| + |\mathcal{E}^b| + |\mathcal{E}_H| + |\mathcal{E}_C|$. Consequently, $\dim V_h^{\mathrm{DG}}(\mathbb{T}) = 2|\mathcal{E}_R| + |\mathcal{E}^b| + |\mathcal{E}_H| + |\mathcal{E}_C| + |\mathbb{T}|$.

On the other hand, $V_h(\mathbb{T})$ differs from $V_h^{\mathrm{DG}}(\mathbb{T})$ by the imposition of $|\mathcal{E}_R| + |\mathcal{E}_C|$ linearly independent constraints. Consequently, $\dim V_h(\mathbb{T}) = \dim V_h^{\mathrm{DG}}(\mathbb{T}) - |\mathcal{E}_R| - |\mathcal{E}_C|$, proving the first claim of the lemma.

The result for the case of $V_{h,0}(\mathbb{T})$ follows immediately from that for $V_h(\mathbb{T})$ by a similar argument, yielding $\dim V_{h,0}(\mathbb{T}) = \dim V_h(\mathbb{T}) - |\mathcal{E}^b|$. This, not coincidentally, also matches the number of dual functionals we have defined in (5.2) and (2.5b). ∎

THEOREM 5.2. *Using the space $V_{h,0}$ defined in* (5.1b)*, the solution of* (4.2) *satisfies the energy norm estimate*

$$|||u - u_h|||_h \le Ch\|u\|_{H^2(\Omega)}.$$

Proof. The proof follows without change from the one given in [12] and outlined in section 4. The key point is that the averages of the solutions on both sides of *child* edges are equal, and consequently the key steps in the estimate of the nonconformity error discussed in section 4 continue to hold. ∎

Let us devote the remainder of this section to a discussion of the constraints we impose in (5.1a). In the context of adaptively refined meshes with hanging nodes, one typically considers two points of view that inform us about theoretical and practical ways to deal with hanging nodes:

- (Global basis functions) The functionals (5.2) and (2.5b) define a basis for $V_{h,0}(\mathbb{T})$ in such a way that there is a basis function φ_e for each edge $e \in (\mathcal{E}_R \cup \mathcal{E}_H)$ and a basis function φ_K for each cell K so that

$$\begin{aligned}
\psi_e(\varphi_{e'}) &= \delta_{e,e'} && \forall e, e' \in (\mathcal{E}_R \cup \mathcal{E}_H),\\
\psi_e(\varphi_K) &= 0 && \forall e \in (\mathcal{E}_R \cup \mathcal{E}_H), K \in \mathbb{T},\\
\psi_K(\varphi_e) &= 0 && \forall e \in (\mathcal{E}_R \cup \mathcal{E}_H), K \in \mathbb{T},\\
\psi_K(\varphi_{K'}) &= \delta_{K,K'} && \forall K, K' \in \mathbb{T}.
\end{aligned}$$

  If the mesh $\mathbb{T}$ has no hanging node, then each of the φ_e has support on exactly the two cells adjacent to the edge e and φ_K has support only on K.
  However, we will show below that if $\mathbb{T}$ does have hanging nodes, the support of basis functions φ_e associated with an edge e may in fact extend beyond the boundaries of the cells adjacent to e. In other words, basis functions are *nonlocal* in the sense that the extent of their support depends not only on the local geometry of the cells adjacent to an edge, but also beyond.
- (Constraints) In implementation practice, one never constructs the global basis functions φ_e and φ_K. Rather, implementations of finite element methods on adaptively refined meshes with hanging nodes almost always define intermediate spaces that *ignore* hanging nodes and then impose additional *constraints* during the assembly and solution process [16, 5, 1]. In the current context, these intermediate spaces would be

$$\widetilde{V}_h(\mathbb{T}) = \left\{ \widetilde{u}_h \in L^2(\Omega) \,\middle|\, \widetilde{u}_h \circ \phi_K \in \widehat{V}\ \forall K \in \mathbb{T}, \right.$$

$$\left. \fint_e [\widetilde{u}_h]_e = 0\ \forall e \in \mathcal{E}_R \right\}, \tag{5.3a}$$

$$\widetilde{V}_{h,0}(\mathbb{T}) = \left\{ \widetilde{u}_h \in \widetilde{V}_h(\mathbb{T}) \,\middle|\, \fint_e \widetilde{u}_h = 0\ \forall e \in \mathcal{E}^b \right\}, \tag{5.3b}$$

with dual functionals

$$\widetilde{\psi}_e(\widetilde{\varphi}_h) = \fint_e \widetilde{\varphi}_h \ \forall e \in \mathcal{E}^i, \tag{5.4}$$

and ψ_K as defined in (2.5b). These spaces and functionals are designed in a way so that one can enumerate degrees of freedom on *every* interior edge, whether it is a regular, further refined, or child edge. In particular, using this viewpoint, one defines a basis function both for each hanging edge as well as its two children.

A function $\widetilde{u}_h = \sum_j \widetilde{U}_j \widetilde{\varphi}_j$ using this basis is then obviously part of $\widetilde{V}_{h,0}(\mathbb{T})$, but not necessarily $V_{h,0}(\mathbb{T})$. To force it into the latter space, one needs to impose constraints

$$\fint_e [\widetilde{u}_h]_e = 0 \qquad \forall e \in \mathcal{E}_C.$$

This condition can be rewritten in terms of the expansion of coefficients $\widetilde{U}_j$:

$$\sum_j C_{ej} \widetilde{U}_j = 0 \qquad \forall e \in \mathcal{E}_C, \tag{5.5}$$

where $(C_{ej}) = \left(\fint_e [\widetilde{\varphi}_j]_e\right)$ is a sparse matrix of size $|\mathcal{E}_C| \times \dim(\widetilde{V}_{h,0})$.

With such constraints in hand, one then builds a (rank deficient) linear system $\widetilde{A}\widetilde{U} = \widetilde{F}$ using the basis for $\widetilde{V}_{h,0}$ and solves it subject to constraint (5.5) to obtain a solution $u_h = \sum_j \widetilde{U}_j \widetilde{\varphi}_j \in V_{h,0}$.

While it is useful to think in terms of the global basis functions φ_j when analyzing a discretization on a mesh with hanging nodes, the point of view of constraints prevails when considering implementing a particular element on such a mesh. This is so because both the assembly of linear systems as well as the computation of the constraint matrix (C_{ej}) is most easily implemented using the basis functions $\widetilde{\varphi}_e, \widetilde{\varphi}_K$: these are the only nonzero basis functions on a cell K, regardless of whether any of the edges e of K is in $\mathcal{E}_C$. Furthermore, knowing (C_{ej}) allows us to construct the basis $\{\varphi_j\}$ from the basis $\{\widetilde{\varphi}_j\}$; see [1]. For these reasons, we will in the following discuss the properties of (C_{ej}) in more detail.

Obviously, (5.5) defines one constraint per child of each hanging edge. As an example, let us consider edge e_{kj} between large cell K_j and child neighbor K_k from Figure 1. Then the constraint that corresponds to this edge reads

$$\fint_{e_{kj}} \left(\widetilde{U}_{e_{kj}} \widetilde{\varphi}_{e_{kj}}\right) = \fint_{e_{kj}} \left(\widetilde{U}_{e_{jk}} \widetilde{\varphi}_{e_{jk}} + \widetilde{U}_{e_{jk}^{\#}} \widetilde{\varphi}_{e_{jk}^{\#}} + \widetilde{U}_{e_{jk}^{+}} \widetilde{\varphi}_{e_{jk}^{+}} + \widetilde{U}_{e_{jk}^{-}} \widetilde{\varphi}_{e_{jk}^{-}} + \widetilde{U}_{K_j} \widetilde{\varphi}_{K_j}\right).$$

By the definition of $\widetilde{\varphi}_{e_{kj}}$, we have that $\fint_{e_{kj}} \widetilde{\varphi}_{e_{kj}} = 1$, and we can rewrite the constraint in the usual form that allows us to eliminate a degree of freedom defined on a child edge in terms of other degrees of freedom using to the following relation:

$$\begin{aligned}
\widetilde{U}_{e_{kj}} = {} & \underbrace{\left[\fint_{e_{kj}} \widetilde{\varphi}_{e_{jk}}\right]}_{=1} \widetilde{U}_{e_{jk}} + \underbrace{\left[\fint_{e_{kj}} \widetilde{\varphi}_{e_{jk}^{\#}}\right]}_{=0} \widetilde{U}_{e_{jk}^{\#}} \\
& + \underbrace{\left[\fint_{e_{kj}} \widetilde{\varphi}_{e_{jk}^{+}}\right]}_{=\frac{1}{4}} \widetilde{U}_{e_{jk}^{+}} + \underbrace{\left[\fint_{e_{kj}} \widetilde{\varphi}_{e_{jk}^{-}}\right]}_{=-\frac{1}{4}} \widetilde{U}_{e_{jk}^{-}} + \underbrace{\left[\fint_{e_{kj}} \widetilde{\varphi}_{K_j}\right]}_{=0} \widetilde{U}_{K_j} \\
= {} & \widetilde{U}_{e_{jk}} + \frac{1}{4}\widetilde{U}_{e_{jk}^{+}} - \frac{1}{4}\widetilde{U}_{e_{jk}^{-}}.
\end{aligned}$$

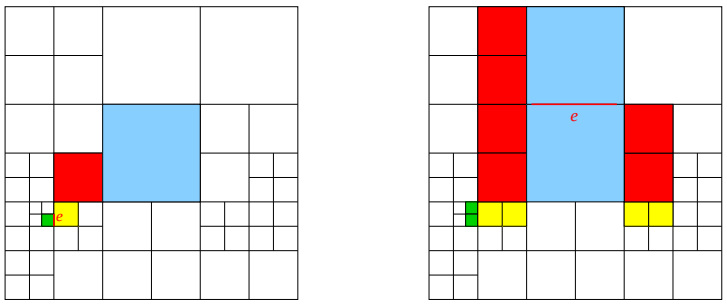

FIG. 2. *Dual points of view for chains of constraints. Left: The coefficient* $\widetilde{U}_e$ *corresponding to a* degree of freedom *defined on an edge* $e \in \mathcal{E}_C$ *may be constrained against a telescoping set of other degrees of freedom. The figure shows the supporting edges and cells of the complete set of degrees of freedom against which* $\widetilde{U}_e$ *is defined. Right: The extended support of the* global basis function φ_e *for one* $e \in \mathcal{E}_R$.

Note that the factors in the first, third, and fourth square brackets on the right are not zero for the DSSY element because, for example, the shape function $\widetilde{\varphi}_{e^+_{jk}}$ has mean value zero on the long edge e_{jk} but not on each of the children e_{kj}, e_{lj} of e_{jk}. This is different from the usual conforming spaces on meshes with hanging nodes where each degree of freedom defined on a child of a hanging edge $e \in \mathcal{E}_C$ is constrained *only in terms of degrees of freedom defined on the parent of* e, but not other parts of the adjacent (large) cell.

This observation is important because, of course, either of the degrees of freedom corresponding to the coefficients $\widetilde{U}_{e^+_{jk}}, \widetilde{U}_{e^-_{jk}}$ may itself lie on the child of a hanging edge and consequently be constrained itself. In other words, in actual computations, we may obtain *chains of constraints*. In order to eliminate the constrained degree of freedom corresponding to the coefficient $\widetilde{U}_{e_{kj}}$ we will therefore have to recursively expand all degrees of freedom that appear on the right-hand side in terms of the degrees of freedom they may be constrained against. This is similar to situations one may find in *hp* adaptive methods in three dimensions (see [1]) and requires the use of more complex data structures and algorithms than one might use for meshes with hanging nodes and "usual" finite elements.[3]

Remark 5.3. The length of these chains of constraints is bounded by the difference between the maximal and minimal generation of cells in $\mathbb{T}$ because it always constrains degrees of freedom on more refined cells against degrees of freedom on less refined neighboring cells. Similarly, the recursive expansion of constraints never leads to circular constraints as long as $\mathbb{T}$ originates from a regular mesh $\mathbb{T}_0$ without hanging nodes as discussed in section 3.

To illustrate the extent to which chains of constraints can expand the support of basis functions, Figure 2 shows both all other degrees of freedom one particular degree of freedom defined on a child edge is constrained against (left), as well as the support of an unconstrained basis function in the basis V_h (right). It is worth pointing

[3]The fact that the constraint weight $[f_{e_{kj}}\, \widetilde{\varphi}_{e^{\#}_{jk}}]$ for the shape function defined on the *opposite* edge of cell K_j happens to be zero is a consequence of putting the hanging node at the midpoint of edge e_{jk}. Had we chosen an unequal subdivision of the edge, the expansion coefficient $\widetilde{U}_{e_{kj}}$ would also be constrained against $\widetilde{U}_{e^{\#}_{jk}}$ with a nonzero weight.

out that to get chains of constraints, it is necessary to have vertices in the mesh with adjacent cells that differ in generation by at least two. On the other hand, widely used mesh smoothing techniques specifically prohibit this, by flagging additional cells for refinement; in these cases, chains of constraints cannot happen as long as refinement bisects edges at the midpoint.

6. Extending the DSSY space to meshes with hanging nodes and edges: Option C. The discussions of the previous section showed that option B for imposing hanging node constraints (see section 4.2) allowed for a trivial extension of the proof of convergence compared to the original one for regular meshes. On the other hand, it leads to constraints that are very different in structure compared to those one typically encounters in conforming finite element methods. This observation motivates us to consider the third option suggested in section 4.2, namely, to require that

$$\frac{1}{2}\left\{ \fint_{e_{kj}} w_h + \fint_{e_{lj}} w_h \right\} = \fint_{e_{jk}} w_h$$

for each hanging edge e_{jk}. In the following subsections, we will theoretically investigate the convergence properties of this approach and then consider the structure of these constraints in analogy to the discussion in the previous section.

6.1. Convergence theory. The formulation of constraints at hanging edges considered in this section implies that $\fint_e [w_h]_e = 0$ for all parent edges $e \in \mathcal{E}_H$, but not the key property $\fint_e [w_h]_e = 0$ for child edges $e \in \mathcal{E}_C$; this property made the convergence proof in the previous section trivial. Nevertheless, we can still show the following result.

THEOREM 6.1. *Let*

$$V_h(\mathbb{T}) = \left\{ u_h \in L^2(\Omega) \,\middle|\, u_h \circ \phi_K \in \widehat{V}\ \forall K \in \mathbb{T}, \quad \fint_e [u_h]_e = 0\ \forall e \in (\mathcal{E}_R \cup \mathcal{E}_H) \right\},$$
$$V_{h,0}(\mathbb{T}) = \left\{ u_h \in V_h(\mathbb{T}) \,\middle|\, \fint_e u_h = 0\ \forall e \in \mathcal{E}^b \right\}.$$

Then the solution of (4.2) *satisfies the energy norm estimate*

$$|||u - u_h|||_h \le Ch\|u\|_{H^2(\Omega)}.$$

As in the case of option B in section 5, it is only necessary to consider the numerator of the consistency error term. It can here be split into the following terms:

$$a_h(u, w_h) - (f, w_h) = -\sum_{e \in \mathcal{E}_R} \langle \mathbf{n}_e \cdot \nabla u, [w_h]_e \rangle_e + \sum_{e \in \mathcal{E}_H} I_e.$$

The terms on regular edges are treated as in the case without hanging nodes, for which we refer to section 4 and [12]. Consequently, we only have to estimate the terms on hanging edges,

$$\begin{aligned} I_{e_{jk}} &= -\left\langle \mathbf{n}_{e_{jk}} \cdot \nabla u, [w_h]_{e_{jk}} \right\rangle_{e_{jk}} \\ &= \left\langle \mathbf{n}_{e_{jk}} \cdot \nabla u, w_h \right\rangle_{e_{jk}} - \left\langle \mathbf{n}_{e_{jk}} \cdot \nabla u, w_h \right\rangle_{e_{kj}} - \left\langle \mathbf{n}_{e_{jk}} \cdot \nabla u, w_h \right\rangle_{e_{lj}}. \end{aligned}$$

As before, $\mathbf{n}_e$ is the normal to edge e with direction consistent with that chosen to define the jump $[w_h]_e$.

To show the result of the theorem, let us define three average values:

$$\overline{\mathbf{g}}_{e_{jk}} = \fint_{e_{jk}} \nabla u, \quad \overline{w}_{e_{jk}} = \fint_{e_{jk}} w_h \quad \text{and } \overline{w}_{e_{kj,lj}} = \frac{1}{2}\left\{ \fint_{e_{kj}} w_h + \fint_{e_{lj}} w_h \right\}.$$

The choice of constraints implies that $\overline{w}_{e_{jk}} = \overline{w}_{e_{kj,lj}}$, or equivalently $\fint_{e_{jk}} [w_h]_{e_{jk}} = 0$, for each hanging edge e_{jk}. Consequently,

$$\begin{aligned}
|I_{e_{jk}}| &= \left| \left\langle \mathbf{n}_{e_{jk}} \cdot (\nabla u - \overline{\mathbf{g}}_{e_{jk}}), [w_h]_{e_{jk}} \right\rangle_{e_{jk}} \right| \\
&= \Bigg| \left\langle \mathbf{n}_{e_{jk}} \cdot (\nabla u - \overline{\mathbf{g}}_{e_{jk}}), \big(w_h - \overline{w}_{e_{jk}}\big) \right\rangle_{e_{jk}} - \left\langle \mathbf{n}_{e_{jk}} \cdot (\nabla u - \overline{\mathbf{g}}_{e_{jk}}), \big(w_h - \overline{w}_{e_{kj,lj}}\big) \right\rangle_{e_{kj}} \\
&\qquad - \left\langle \mathbf{n}_{e_{jk}} \cdot (\nabla u - \overline{\mathbf{g}}_{e_{jk}}), \big(w_h - \overline{w}_{e_{kj,lj}}\big) \right\rangle_{e_{lj}} \Bigg| \\
&\le \left\| \nabla u - \overline{\mathbf{g}}_{e_{jk}} \right\|_{0,e_{jk}} \left\| w_h - \overline{w}_{e_{jk}} \right\|_{0,e_{jk}} \\
&\qquad + \left(\sum_{\iota \in \{k,l\}} |e_{\iota j}| \left\| \nabla u - \overline{\mathbf{g}}_{e_{jk}} \right\|^2_{0,e_{\iota j}} \right)^{1/2} \left(\sum_{\iota \in \{k,l\}} |e_{\iota j}|^{-1} \left\| w_h - \overline{w}_{e_{kj,lj}} \right\|^2_{0,e_{\iota j}} \right)^{1/2}.
\end{aligned}$$

The difficulty to overcome here is that in the last term, $w_h - \overline{w}_{e_{kj,lj}}$ does not have mean value zero over the child edge $e_{\iota j}, \iota \in \{k,l\}$ we integrate over and consequently does not provide us with the necessary power of the mesh size.

For the following, let us denote the diameter of the element $K \in \mathbb{T}$ and of the edge $e \in \mathcal{E}$ by h_K and h_e, respectively. Then the following three auxiliary estimates hold from essential interpolation estimates (the first one mirroring (4.5a)):

$$\begin{aligned}
\left\| \nabla u - \overline{\mathbf{g}}_{e_{jk}} \right\|_{0,e_{jk}} &\le C h^{1/2}_{e_{jk}} \|u\|_{2,K_j}, \\
\left\| w_h - \overline{w}_{e_{jk}} \right\|_{0,e_{jk}} &\le C h^{1/2}_{e_{jk}} |w_h|_{1,K_j}, \\
\left(\sum_{\iota \in \{k,l\}} h_{e_{\iota j}} \left\| \nabla u - \overline{\mathbf{g}}_{e_{jk}} \right\|^2_{0,e_{\iota j}} \right)^{1/2} &\le C \left(\sum_{\iota \in \{k,l\}} h^2_{e_{\iota j}} \|u\|^2_{2,K_\iota} \right)^{1/2}.
\end{aligned}$$

The main difficulty of the error analysis is to show the following lemma.

LEMMA 6.2.

$$\left(\sum_{\iota \in \{k,l\}} h^{-1}_{e_{\iota j}} \left\| w_h - \overline{w}_{e_{kj,lj}} \right\|^2_{0,e_{\iota j}} \right)^{1/2} \le C \left(\sum_{\iota \in \{k,l\}} |w_h|^2_{1,K_\iota} \right)^{1/2}. \tag{6.1}$$

For the proof of this lemma, let us first introduce some notation and auxiliary results. To this end, let

$$\widehat{K}_k := [0,1] \times [0,1], \qquad \widehat{K}_l := [0,1] \times [-1,0]$$

be the two reference squares and $\mathbf{F}_\iota : \widehat{K}_\iota \longrightarrow K_\iota$ be the bilinear transformation onto K_ι for $\iota \in \{k,l\}$. See Figure 3 for illustration. Then the piecewise bilinear transformation $\mathbf{F}$ is defined by

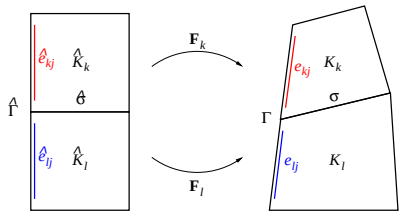

FIG. 3. *Piecewise bilinear mappings* $\mathbf{F}_\iota : \widehat{K}_\iota \longrightarrow K_\iota, \iota \in \{k,l\}$, *between the reference squares and genuine quadrilaterals.*

$$\mathbf{x} = \mathbf{F}(\widehat{\mathbf{x}}) := \begin{cases} \mathbf{F}_k(\widehat{\mathbf{x}}), & \widehat{\mathbf{x}} \in \widehat{K}_k, \\ \mathbf{F}_l(\widehat{\mathbf{x}}), & \widehat{\mathbf{x}} \in \widehat{K}_l. \end{cases}$$

It is useful to define the combined reference domain $\widehat{K}_{kl} := \widehat{K}_k \cup \widehat{K}_l$ and the associated domain $K_{kl} := K_k \cup K_l$. Denote by $\widehat{e}_{\iota j}$ the edge of $\widehat{K}_\iota$ associated with $e_{\iota j}$ for $\iota \in \{k,l\}$ and by $\widehat{\sigma}$ the edge common to $\widehat{K}_k$ and $\widehat{K}_l$. We will designate by $\widehat{\Gamma} = \{0\} \times [-1,1]$ the part of the boundary of $\widehat{K}_{kl}$. σ and Γ will mean the images under $\mathbf{F}$ of $\widehat{\sigma}$ and $\widehat{\Gamma}$, respectively. Geometrically, Γ is identical to e_{jk} and e_{jl} in Figure 1.

We invoke the following standard results derived using shape regularity of $\mathbb{T}$.

LEMMA 6.3. *There exist constants* $c, C > 0$ *such that, for every element* $K \in \mathbb{T}$,

$$ch_K^2 \le \det \left| \frac{\partial \mathbf{x}}{\partial \widehat{\mathbf{x}}} \right| \le Ch_K^2, \tag{6.2a}$$

$$\left| \frac{\partial x_m}{\partial \widehat{x}_n} \right| \le Ch_K, \quad m,n = 1,2. \tag{6.2b}$$

LEMMA 6.4. *For given* $w_h \in V_{h,0}(\mathbb{T})$, *define* $\widehat{w}_h := w_h|_{K_{kl}} \circ \mathbf{F} \in L^2(\widehat{K}_{kl})$. *Then, the following statements hold:*

$$1. \quad \fint_{\widehat{\sigma}} [\widehat{w}_h]_{\widehat{\sigma}} = 0, \qquad 2. \quad \fint_{\widehat{\Gamma}} \widehat{w}_h = \overline{w}_{e_{kj,lj}}.$$

We are now ready to prove Lemma 6.2. Trace and Poincaré–Friedrichs inequalities for piecewise H^1 functions on the reference domains [2] imply that we can estimate as follows:

$$\begin{aligned}
&\sum_{\iota \in \{k,l\}} h_{e_{\iota j}}^{-1} \left\| w_h - \overline{w}_{e_{kj,lj}} \right\|_{0,e_{\iota j}}^2 \le C \left[\left\| \widehat{w}_h - \overline{w}_{e_{kj,lj}} \right\|_{0,\widehat{e}_{kj}}^2 + \left\| \widehat{w}_h - \overline{w}_{e_{kj,lj}} \right\|_{0,\widehat{e}_{lj}}^2 \right] \\
&\quad \le C \left[\left\| \widehat{w}_h - \overline{w}_{e_{kj,lj}} \right\|_{0,\widehat{K}_k}^2 + \left| \widehat{w}_h - \overline{w}_{e_{kj,lj}} \right|_{1,\widehat{K}_k}^2 + \left\| \widehat{w}_h - \overline{w}_{e_{kj,lj}} \right\|_{0,\widehat{K}_l}^2 + \left| \widehat{w}_h - \overline{w}_{e_{kj,lj}} \right|_{1,\widehat{K}_l}^2 \right] \\
&\quad = C \left[\left\| \widehat{w}_h - \overline{w}_{e_{kj,lj}} \right\|_{0,\widehat{K}_{kl}}^2 + \sum_{\iota \in \{k,l\}} \left| \widehat{w}_h - \overline{w}_{e_{kj,lj}} \right|_{1,\widehat{K}_\iota}^2 \right] \\
&\quad \le C \left[\sum_{\iota \in \{k,l\}} \left| \widehat{w}_h - \overline{w}_{e_{kj,lj}} \right|_{1,\widehat{K}_\iota}^2 + \left(\int_{\widehat{\sigma}} [\widehat{w}_h - \overline{w}_{e_{kj,lj}}]_{\widehat{\sigma}} \, \mathrm{d}\widehat{s} \right)^2 + \left(\int_{\widehat{\Gamma}} \widehat{w}_h - \overline{w}_{e_{kj,lj}} \, \mathrm{d}\widehat{s} \right)^2 \right] \\
&\quad = C \sum_{\iota \in \{k,l\}} |\widehat{w}_h|_{1,\widehat{K}_\iota}^2 \le C \sum_{\iota \in \{k,l\}} |w_h|_{1,K_\iota}^2 .
\end{aligned}$$

This proves Lemma 6.2. It is worth noting that the inequality constant in the proof depends on the shape regularity of $\mathbb{T}$ only.

All of this together now also allows us to finish the proof of Theorem 6.1. With the above lemmas, we obtain

$$|I_{e_{jk}}| \le C \left[h_{e_{jk}} \|u\|_{2,K_j} |w_h|_{1,K_j} + \left(\sum_{\iota\in\{k,l\}} h_{e_{\iota j}}^2 \|u\|_{2,K_\iota}^2 \right)^{1/2} \left(\sum_{\iota\in\{k,l\}} |w_h|_{1,K_\iota}^2 \right)^{1/2} \right]$$
$$\le C \left(\sum_{K\in\omega(e_{jk})} \|h_K u\|_{2,K}^2 \right)^{1/2} \left(\sum_{K\in\omega(e_{jk})} |w_h|_{1,K}^2 \right)^{1/2},$$

where $\omega(e_{jk}) = \{K_j, K_k, K_l\}$ is the set of elements containing all or parts of e_{jk} as an edge. This yields the following, order-optimal bound for the consistency error:

$$\sup_{w_h\in V_h} \frac{a_h(u,w_h) - (f,w_h)}{|||w_h|||_h} \le C \left(\sum_{K\in\mathbb{T}} \|h_K u\|_{2,K}^2 \right)^{1/2}.$$

6.2. Structure of the constraints. The constraints discussed in this section only couple degrees of freedom on the hanging, parent edge and its children, but not those defined on adjacent edges or the interior of cells. This is different from the constraints of the previous section; in particular, we no longer have to deal with chains of constraints.

Using the approach of the current section, we have only one constraint per hanging edge that contains the degrees of freedom for *both* child edges. Conceptually, this can be interpreted as constraining the degree of freedom *on the parent edge* against those on all children, a reversal of the situation for conforming elements where we constrain the degrees of freedom on each child edge separately against those on the parent edge. Other than the fact that this does not follow the "usual" pattern, implementing these constraints in software does not present any undue burdens.

6.3. A comparison with the other options. Proving optimal convergence order for option C required showing that the set of functions satisfying the constraints (4.8) yields optimal order for the nonconformity error, $\sup_{w_h\in V_h} \frac{a_h(u,w_h)-(f,w_h)}{|||w_h|||_h}$, in (4.4). On the other hand, comparing (4.8) with (4.6) and (4.7) shows that functions that satisfy constraint options A and B *also satisfy the constraints of option C*. In other words, the function spaces defined by options A and B are *smaller* than those of option C. It is then obvious that the nonconformity error must also be of optimal order for options A and B.

On the other hand, we will show experimentally in the next section that option A does not converge. This is because for this option, the best-approximation term in (4.4) is not of optimal order. This is easy to see: globally linear functions are not in the discrete space defined by constraint (4.6) if hanging nodes are present.

7. Numerical results. In this section, we will numerically evaluate the performance of the three options to impose constraints for the DSSY element outlined in section 4.2. As proven in sections 5 and 6, the second and third options yield convergent schemes of optimal order, but it is unclear which one may be better in absolute terms. We here investigate this question numerically and also show that the first option to define constraints does not yield a scheme that converges in the energy norm.

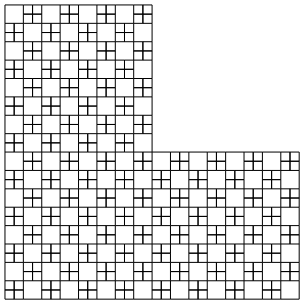

FIG. 4. *A mesh with the maximal number of hanging nodes. Here, every interior edge contains a hanging node.*

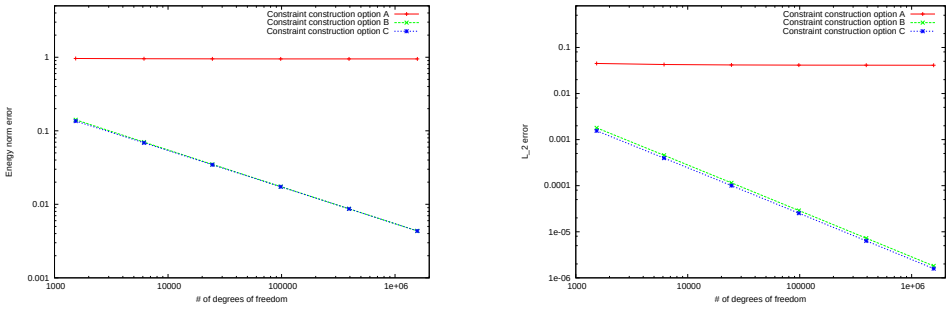

FIG. 5. *Maximally bad meshes, smooth solution: Convergence of the solution u_h toward the exact solution u on a sequence of meshes with the maximal number of hanging nodes, using the three different options to construct constraints discussed in section* 4.2. *Left: The energy norm error $|||u - u_h|||_h$. Both options* B *and* C *yield a convergence order of $\mathcal{O}(N^{-1/2}) = \mathcal{O}(h)$. Right: The L_2 norm error $\|u - u_h\|_0$, converging as $\mathcal{O}(N^{-1}) = \mathcal{O}(h^2)$.*

7.1. Maximally bad meshes, smooth solution. The worst mesh as far as hanging nodes are concerned is one in which every other cell is refined, starting from a uniformly refined mesh; see Figure 4.

We first investigate the convergence of the numerical solution using a test case with the smooth exact solution $u = \cos(\pi x)\cos(\pi y)$ on the L-shaped domain $\Omega = (-\frac{1}{2}, \frac{1}{2})^2 \backslash [0, \frac{1}{2}]^2$. Figure 5 shows both the energy and L_2 norm errors for the three options of imposing hanging node constraints. Options B and C both show optimal order convergence in both norms, and the errors are in fact not substantially different.

Option A does not converge in either norm. The fact that it does not converge in the energy norm may not be surprising: Figure 6 shows the solution (for the nonsmooth test case discussed in the next section) and demonstrates that requiring the values along both child edges to be the same yields a tilted numerical solution whenever the derivative of the exact solution in the direction of the edge is nonzero. Consequently, the gradient of the numerical solution does not converge to that of the exact solution. That the L_2 norm does not converge at any appreciable rate (it does decrease very slowly) is more surprising. A closer investigation shows that the numerical solution is consistently smaller than the exact one, suggesting that the imposition of these constraints leads to a discrete problem that is too rigid.

For the mesh used in the current section, constraints are not chained because no cell has both hanging edges and edges that are children of hanging edges of other

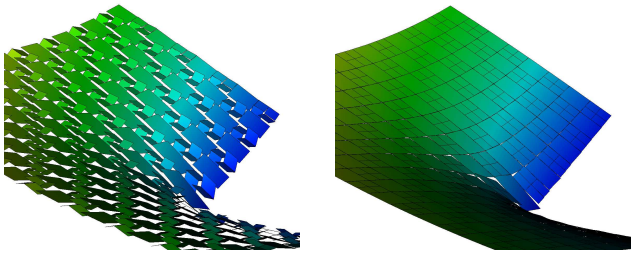

FIG. 6. *Maximally bad meshes, singular solution: Solutions on the same mesh using options* A *(left) and* C *(right) for the imposition of constraints. The solution for option* B *looks essentially the same as the picture on the right, with only marginal visible differences for the cells at the reentrant corner. Color and elevation both show the value of* $u_h(\mathbf{x})$ *at a point* $\mathbf{x} \in \Omega$.

cells. Nonetheless, the three different options of dealing with hanging nodes yield very different constraints that, if resolved, yield matrices with different numbers of nonzero entries. To illustrate this, consider a mesh similar to the one in Figure 4 but refined four more times globally before refining every other cell. The associated finite element space has 393,216 degrees of freedom before eliminating constrained ones. The three options of constructing constraints then yield matrices with 2,651,130, 4,996,106, and 3,236,864 entries in the sparsity pattern.[4] While we know that option A is not viable, option B results in a matrix with about 50% more entries than option C. Consequently, solvers will typically also require more CPU time using this approach.

7.2. Maximally bad meshes, singular solution. A more interesting test case is to solve a problem with a singular solution on such maximally bad meshes. We again use the L-shaped domain introduced above and choose right-hand-side and boundary values in such a way that we reproduce an exact solution that in polar coordinates reads

$$u(r,\theta) = r^{\frac{2}{3}} \sin\left(\frac{2}{3}\left(\theta - \frac{\pi}{2}\right)\right), \qquad \frac{\pi}{2} \le \theta \le 2\pi.$$

The numerical solutions for options A and C for the imposition of constraints are shown in Figure 6. The fact that for option A all small cells are tilted to accommodate the constraint that the average values on both child edges are equal explains why we do not see convergence in the energy norm. (A similar picture, though far less obvious, could also have been made for the previous example.)

Given the singularity at the origin, we cannot expect to obtain optimal convergence orders. Indeed, as shown in Figure 7, the convergence order is reduced. Options B and C do not differ in noticeable ways in energy norm. There is a small difference in the L_2 norm whose origin we have not been able to elucidate; in particular, the convergence order for option B depends on whether the checkerboard mesh is created by refining the "white" fields ($\mathcal{O}(h^{1.62})$) or the "black" fields ($\mathcal{O}(h^{1.5})$), whereas option C does not show any difference in this regard.

7.3. Fully adaptive meshes, singular solution. We conclude our numerical experiments by comparing results obtained for the singular solution test case above, but using meshes that are generated by an a posteriori error estimator that takes

[4] We have verified that asymptotically, the number of entries in the sparsity pattern and the number of nonzero entries in the matrix are the same.

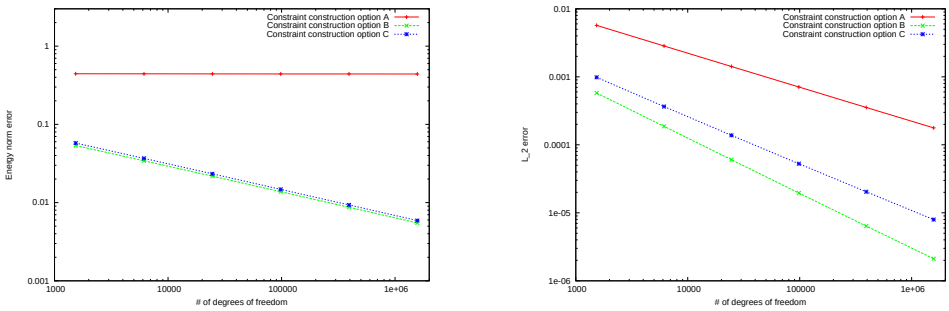

FIG. 7. *Maximally bad meshes, singular solution: Convergence of the solution u_h toward the exact solution u on a sequence of meshes with the maximal number of hanging nodes, using the three different options to construct constraints discussed in section* 4.2. *Left: The energy norm error $|||u - u_h|||_h$. Both options* B *and* C *yield a convergence order of $\mathcal{O}(N^{-1/3}) = \mathcal{O}(h^{2/3})$. Right: The L_2 norm of the error. Here, option* B *yields a convergence order of $\mathcal{O}(N^{-0.81}) = \mathcal{O}(h^{1.62})$ and option* C *a convergence order of $\mathcal{O}(N^{-0.69}) = \mathcal{O}(h^{1.38})$. Option* A*, which does not converge in the energy norm, still yields a convergence order of $\mathcal{O}(N^{-0.5}) = \mathcal{O}(h^1)$ in the L_2 norm.*

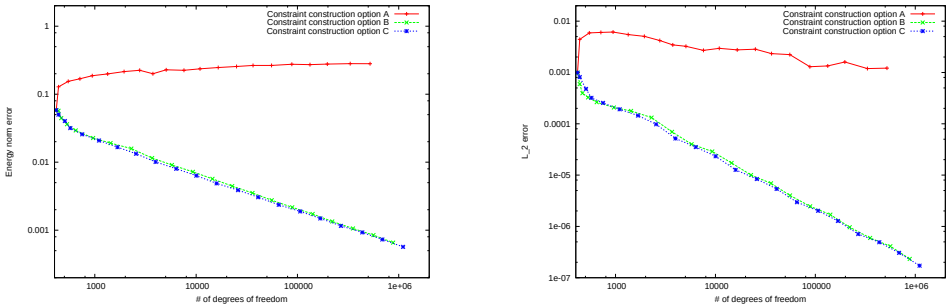

FIG. 8. *Fully adaptive meshes meshes, singular solution: Convergence of the solution u_h toward the exact solution u on a sequence of adaptively refined meshes, using the three different options to construct constraints discussed in section* 4.2. *Left: The energy norm error $|||u - u_h|||_h$. Option* B *yields a convergence order of $\mathcal{O}(N^{-0.51})$ and option* C *a convergence order of approximately $\mathcal{O}(N^{-0.5})$. Right: The L_2 norm of the error. Both options* B *and* C *yield a convergence order of approximately $\mathcal{O}(N^{-1})$.*

into account both the residuals of the discrete solution as well as the nonconformity [8, 7, 10]. Because the first option for enforcing constraints yields a solution that violates the assumptions underlying the error estimator, we obtain nonsensical meshes, and therefore omit this approach from the current section. The generated meshes obtained from options B and C show the expected refinement toward the reentrant corner where the solution is singular and have the familiar appearance for such meshes.

Figure 8 shows the convergence history for all approaches. Both options B and C yield essentially the same errors. Finally, we show in Figure 9 the growth in the number of nonzero entries in the system matrix after application of constraints. This is relevant because, unlike the examples on the meshes of the previous subsections, the current mesh consists of cells on many levels; consequently, option B may generate chains of constraints that have the potential to create many more nonzeros in the matrix. In fact, one can construe sequences of meshes in which the number of nonzeros grows *faster* than $\mathcal{O}(N)$ where N is the number of degrees of freedom. On the other hand, the figure shows that in practice, the number of nonzeros averages around 7 per

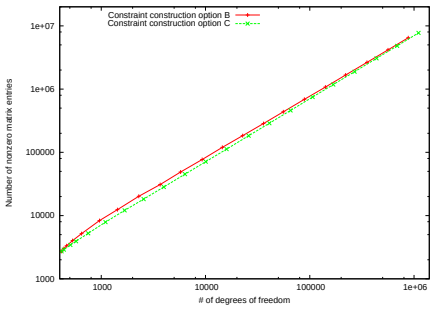

FIG. 9. *Fully adaptive meshes meshes, singular solution: Number of nonzero entries in the matrix as a function of the number of unknowns in the problem.*

row for option C, and slightly greater than 7 for option B. In other words, there is no noticeable difference in computational cost between the two approaches. This can be explained by the fact that on typical, adaptively refined meshes, few hanging edges give rise to long constraint chains such as those shown in Figure 2. In fact, in our computations, we had no cases of chained constraints at all, since no vertices existed with neighboring cells whose refinement levels differed by two or more.

8. Conclusions. For nonconforming finite element methods, the construction of hanging node constraints is not as obvious as for conforming methods. In this paper, we have presented a number of options for how hanging nodes can be treated for one nonconforming element, namely, the DSSY element. We identified two different strategies—both rather different from the structure of constraints typically encountered for conforming methods—for which we could prove theoretically that they converge, and also demonstrate this using numerical experiments. They differ in their implementation complexity, but not substantially in the accuracy they yield.

We expect that considerations similar to those discussed herein can also guide the derivation of constraints for other nonconforming elements, as well as for hanging nodes generated by independent refinements [3].

REFERENCES

[1] W. BANGERTH AND O. KAYSER-HEROLD, *Data structures and requirements for hp finite element software*, ACM Trans. Math. Software, 36 (2009), pp. 4/1–4/31.

[2] S. BRENNER AND R. SCOTT, *The Mathematical Theory of Finite Element Methods*, Texts in Appl. Math., 15, Springer, New York, 2007.

[3] S. BRENNER AND L.-Y. SUNG, *Piecewise H^1 functions and vector fields associated with meshes generated by independent refinements*, Math. Comp., 84 (2015), pp. 1017–1036.

[4] Z. CAI, J. DOUGLAS, JR., J. E. SANTOS, D. SHEEN, AND X. YE, *Nonconforming quadrilateral finite elements: A correction*, Calcolo, 37 (2000), pp. 253–254.

[5] G. F. CAREY, *Computational Grids: Generation, Adaptation and Solution Strategies*, Taylor & Francis, New York, 1997.

[6] C. CARSTENSEN AND J. HU, *A unifying theory of a posteriori error control for nonconforming finite element methods*, Numer. Math., 107 (2007), pp. 473–502.

[7] C. CARSTENSEN AND J. HU, *Hanging nodes in the unifying theory of a posteriori finite element error control*, J. Comput. Math, 27 (2009), pp. 215–236.

[8] C. CARSTENSEN, J. HU, AND A. ORLANDO, *Framework for the a posteriori error analysis of nonconforming finite elements*, SIAM J. Numer. Anal., 45 (2007), pp. 68–82.

[9] M. CROUZEIX AND P.-A. RAVIART, *Conforming and nonconforming finite element methods for solving the stationary Stokes equations*, RAIRO Math. Model. Numer. Anal., R-3 (1973), pp. 33–75.

[10] E. Dari, R. Duran, C. Padra, and V. Vampa, *A posteriori error estimators for nonconforming finite element methods*, RAIRO Math. Model. Numer. Anal., 30 (1996), pp. 385–400.

[11] A. Dedner, R. Klöfkorn, and M. Kränkel, *Continuous finite-elements on non-conforming grids using discontinuous Galerkin stabilization*, in Proceedings of Finite Volumes for Complex Applications VII—Methods and Theoretical Aspects, Springer Proc. Math. Statist., 77, Springer, New York, 2014, pp. 207–215.

[12] J. Douglas, Jr., J. E. Santos, D. Sheen, and X. Ye, *Nonconforming Galerkin methods based on quadrilateral elements for second order elliptic problems*, ESIAM Math. Model. Numer. Anal., 33 (1999), pp. 747–770.

[13] F. Huang and X. Xie, *A modified nonconforming* 5*-node quadrilateral transition finite element*, Adv. Appl. Math. Mech., 2 (2010), pp. 784–797.

[14] Y. Jeon, H. Nam, D. Sheen, and K. Shim, *A class of nonparametric DSSY nonconforming quadrilateral elements*, ESAIM Math. Model. Numer. Anal., 47 (2013), pp. 1783–1796.

[15] R. Rannacher and S. Turek, *Simple nonconforming quadrilateral stokes element*, Numer. Methods Partial Differential Equations, 8 (1992), pp. 97–111.

[16] W. C. Rheinboldt and C. K. Mesztenyi, *On a data structure for adaptive finite element mesh refinements*, ACM Trans. Math. Software, 6 (1980), pp. 166–187.

[17] W. Schmid, *Adaptive gemischte und nichtkonforme Finite-Elemente Methoden und Anwendungen auf die Mehrgruppen-Diffusionsgleichungen*, Ph.D. thesis, University of Augsburg, Germany, 1996.

[18] W. Schmid and F. Wagner, *Numerical solution of the neutron diffusion equation—adaptive concepts in time and space*, in Numerical Treatment of Coupled Systems, Notes Numer. Fluid Mech. 51, Springer, Berlin, 1995, pp. 163–174.

[19] P. Šolín, J. Červený, and I. Doležel, *Arbitrary-level hanging nodes and automatic adaptivity in the hp-FEM*, Math. Comput. Simulation, 77 (2008), pp. 117–132.

[20] P. Šolín, K. Segeth, and I. Doležel, *Higher-Order Finite Element Methods*, Chapman & Hall/CRC, London, 2003.

[21] G. Strang, *Variational crimes in the finite element method*, in The Mathematical Foundations of the Finite Element Method with Applications to Partial Differential Equations, A. K. Aziz, ed., Academic Press, New York, 1972, pp. 689–710.